Contrib. Astron. Obs. Skalnaté Pleso **49**, 246 – 251, (2019)

KOREL disentangling of the LMC eclipsing Algol OGLE-LMC-DPV-065

M. Cabezas[1], P. Hadrava[1], R. E. Mennickent[2] and T. Rivinius[3]

[1] *Astronomical Institute of the Czech Academy of Sciences Boční II 1401, 141 31 Praha 4, Czech Republic*

[2] *Departamento de Astronomía, Universidad de Concepción Casilla 160-C, Concepción, Chile*

[3] *ESO - European Organisation for Astronomical Research in the Southern Hemisphere, Casilla 19001, Santiago 19, Chile*

Received: November 1, 2018; Accepted: March 8, 2019

Abstract. We present disentangled orbital parameters and component spectra of the double-periodic eclipsing Algol OGLE-LMC-DPV-065. Direct spectroscopic evidence on a disk-like envelope around the primary star and circumstellar matter in the system is given.

Key words: spectroscopic – binary stars – disentangling – eclipsing binary

1. Introduction

A group of hot Algols shows a long photometric cycle with average about 33 times its orbital period. This group is called Double Periodic Variables (DPVs, Mennickent et al., 2003, 2016, 2017, Poleski et al. 2010). DPVs are semidetached binaries typically consisting of an A/F/G giant star filling its Roche lobe and transferring mass onto a B-type primary surrounded by a circumprimary disk.

The OGLE-LMC-DPV-065 (R.A.$_{2000}$ = 05:20:04.07, Dec.$_{2000}$ = -69:36:39.1; OGLE05200407-6936391) is one of the brightest DPVs in LMC (V =14.74, $B - V = -0.07$), with an orbital period of $P_o = 10^d.031645 \pm 0.000033$ (Poleski et al., 2010). This is an interesting target because the system is eclipsing and shows a change in the long period: from 340 to 210 days in 15 years. In this work we present its orbital solution and the separated spectra obtained using the method of disentangling of spectra.

2. Observations

Our spectroscopic data consist of 27 exposures obtained in overall time of 25 hours of observations in the service mode with the ESO Ultraviolet and Visual Echelle Spectrograph UVES (Dekker et al., 2000) at the Kueyen telescope in the Paranal Observatory. This is a cross-dispersed echelle spectrograph in which the light beam is split into two main spectral regions; the Blue region, covering 3760-4985 Å, and the Red region, covering 5700-7520 Å. This instrument provides an accurate calibration of the wavelength scale close to 50 m/s and a resolving power of 50 000 and 55 000, respectively, for each region.

In this work we use seven spectral regions containing metallic lines which are not blended and are much narrower than other lines such as those of H and He. To diminish the numerical errors of disentangling we have used an oversampling (compared to the spectrograph resolution and pixel-size of the original detector) of each spectral region in 4096 bins and an average resolution of RV/bin=0.7256 $\mathrm{km\,s^{-1}}$. The details about preparation of the data and operation of the `KOREL` code can be found at the User's guide (Hadrava, 2004b).

3. Results

3.1. Solution of orbital parameters

In order to obtain the radial velocities and orbital parameters we used the `KOREL` code which directly yields also the separated spectra of the components of a multiple stellar system under study. Four solutions of orbital parameters are presented in Table 1. The period was fixed in all of them to $P_o = 10.0316267$ days found from a combination of various photometric data sets. The periastron epoch τ^* given in Table 1 is HJD–2453300.

Table 1. Summary of our different solutions.

Parameter	I	II	III	IV
τ^*	92.31±0.02	92.305±0.004	94.79±0.33	92.35±0.14
K_1 [$\mathrm{km\,s^{-1}}$]	42.60±0.97	42.44±0.33	42.45±0.32	42.92±0.38
K_2 [$\mathrm{km\,s^{-1}}$]	210.5±6.4	214.1±1.8	213.5±1.7	209.1±1.8
q	0.203±0.008	0.198±0.002	0.199±0.002	0.205±0.002
ω [deg]	90	90	178.7±11.6	90
e	0	0	0.021±0.006	0

The first three solutions are based on the same above-described seven spectral regions. Solution I corresponds to the average of the seven `KOREL`-solutions calculated for each spectral region independently. The errors of the parameters are the standard deviations. Solution II is the best fit obtained using the `KOREL` for the multiregion data, that is with all the seven spectral regions as input fitted simultaneously. In this procedure we do not get directly errors of the parameters, but we can find their Bayesian estimate (cf. Hadrava, 2016) using the outputs of `KOREL` which map the χ^2 in two-dimensional cross-sections of the parameter space for each pair of parameters. The above mentioned oversampling of the input data must be taken into account to find the proper number of statistically independent pixels of noise. The errors of the parameters and their correlation coefficients (e.g. $c_{K_1,q} = 0.972$ for the Solution II) can then be calculated from the moments of the Bayesian probability distribution. Another possibility to estimate the errors of disentangled parameters is to compare them with a solution of radial-velocity curves obtained, e.g., using FOTEL (cf. Hadrava, 2004a) from the radial velocities calculated by KOREL. It should be, however, noted that the usually given error-bars of published values of parameters yield anyway only very limited information about their uncertainties. For instance, the (Bayesian-probability) weighted mean values (e.g. $\bar{K}_1 = 42.38\ \mathrm{km\,s^{-1}}$ in the $\{K_1, q\}$-plane of Solution II) generally differ from the values at the deepest minima of χ^2 which may be influenced by an interference of the noise and there may exist several comparable solutions. The inspection of the probability distribution thus yields more reliable information. In both solutions I and II we considered a circular orbit, i.e. we fixed $e = 0$ and $\omega = 90°$.

Table 2. Systemic velocities measured from individual lines.

Spectral line Å	γ_{pri} $\mathrm{km\,s^{-1}}$	Spectral line Å	γ_{pri} $\mathrm{km\,s^{-1}}$	Spectral line Å	γ_{sec} $\mathrm{km\,s^{-1}}$
He I 4143.76	279.22	Si II 4621.42	271.29	Si II 4128.05	281.14
N II 4227.74	276.36	O II 4638.85	276.56	Si II 4130.89	278.43
N II 4236.91	277.24	O II 4641.81	276.86	Fe II 4233.17	280.48
N II 4241.78	272.03	O II 4649.14	276.16	Cr II 4242.36	275.77
O II 4414.88	275.35	O II 4699.21	270.56	Sc II 4246.82	275.29
O II 4416.97	274.26	O II 4705.36	276.68	Ti II 4443.79	277.68
He I 4437.55	276.15	He I 4713.14	278.23	Ti II 4533.96	281.19
N II 4447.04	273.91			Ti II 4549.62	284.99
Si III 4567.84	276.48			Cr II 4558.65	277.75
Si III 4574.76	274.98			Ti II 4563.76	281.19
O II 4590.97	274.64			Ti II 4571.97	282.47
O II 4596.17	273.44			Fe II 4629.34	278.68
N II 4607.15	272.24			Fe II 4731.45	280.79

The Solution III is similar to the Solutions II, but it takes into account a possible eccentricity of the orbit (i.e. $e \neq 0$). The best fit to the multiregion data given in the Solution III indicates a slight asymmetry of the radial-velocity curve corresponding to the eccentricity 0.021. The Bayesian probability distribution in the plane of e and the correlated τ and ω is, however, very irregular and the mean value of the eccentricity $\bar{e} = 0.017$. The periastron longitude is close to 180°, so that the eccentricity should be also seen in photometry. However, our FOTEL-solution of the OGLE-photometry (Poleski et al., 2010) limits the eccentricity to 0.0007 ± 0.01. In view of the long-term variability of the system, which indicates the presence of some circumstellar matter, the asymmetry may be due to some other reasons and the marginal evidence for the eccentricity in the currently available data cannot be accepted as real.

In addition to the seven spectral regions containing the narrow 'metal' lines suitable for determination of the orbital parameters we also disentangled the Hα region. The corresponding results are given as the Solution IV. The Hα line is

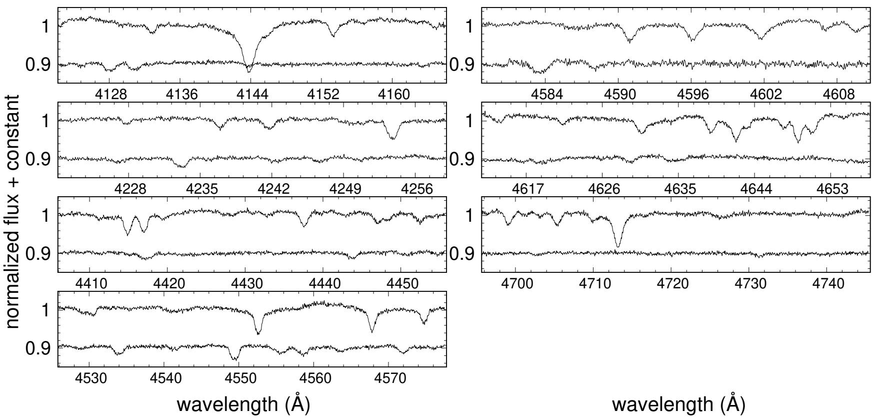

Figure 1. The component spectra in our seven selected regions disentangled using KOREL. For each panel the upper spectrum corresponds to the primary component and the lower spectrum to the secondary component. The wavelength scale is shifted for the mean γ-velocity to correspond to the laboratory wavelengths of the lines.

highly influenced by the circumstellar matter, which may distort the line profiles (as it will be discussed in Section 3.3). In the following we shall thus adopt the Solution II as the most reliable information on the orbital parameters.

The procedure of disentangling does not need any identification of spectral lines and in fact it uses the disentangled mean component spectra as a template to find the changes of radial velocities in the individual exposures. To find the systemic velocity, i.e. the radial velocity of the center of mass of the binary system, we thus adopted an average of radial velocities calculated by Gaussian adjustments for different spectral lines in each disentangled component spectrum shown in Table 2. We arrived at mean values $\gamma_{pri} = 275.1 \pm 2.3$ km s^{-1} for the primary and $\gamma_{sec} = 279.6 \pm 2.8$ km s^{-1} for the secondary component.

3.2. Disentangled spectra

Figure 1 shows the seven selected regions. As we can see, the first component, which is hotter, has strong lines of He I, N II, O II, and Si II. In turn, the colder component has metallic weak lines of Fe II, Si II, Cr II, and Ti II. The separation of these spectra is crucial for our future study in which we plan to determine the spectral type of each component and its physical parameters.

3.3. H$_\alpha$ region

To study the circumstellar matter in the system we also disentangled the region of H$_\alpha$ line. This region is highly contamined by the telluric water-vapour lines, so

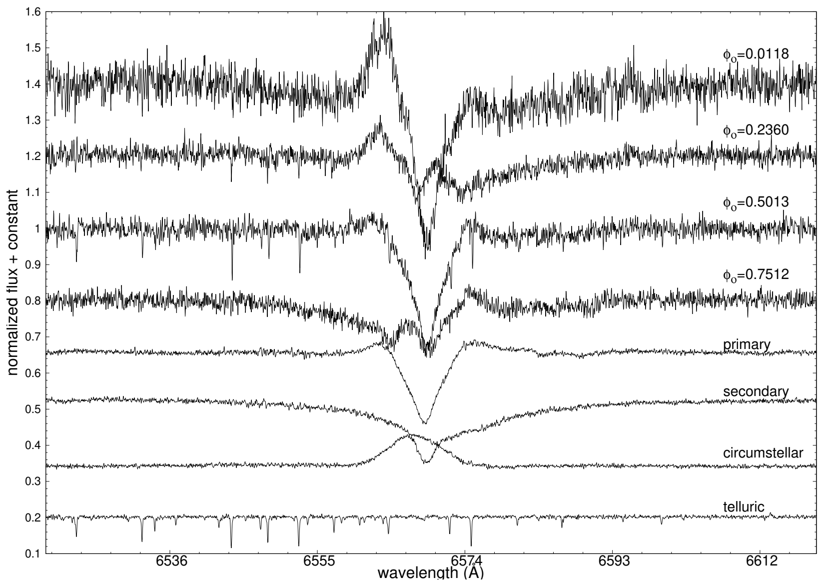

Figure 2. Spectra of DPV 065 in the Hα region. From the top: observed spectra at four different phases, separated spectra of the primary and secondary component, emission of the circumsetallar matter and the telluric lines.

it is advantageous to add into the disentangling also a component moving with the annual motion of the Earth. If we disentangled the region with the three components for the two stars and the tellurics, we arrived at orbital parameters within errors equal to the Solution II; the shape of the disentangled spectra was qualitatively similar to the corresponding component spectra shown in Figure 2. The primary component has a double-peak emission in wings which suggests a disk-shaped envelope. While in the previous solutions of the narrow-line regions the line strengths of the primary component were diminished and those of the secondary enhanced in the exposure taken close to the primary minimum, in the Hα region the emission is enhanced in this phase (in particular in the blue wing – see the top spectrum in Figure 2). Generally, the fit of Hα profile was not much precise and residuals in all phases contained humps revealing inhomogeneities in the circumstellar matter. To improve the fit we included into the disentangling a third component corrotating with the binary with an unknown phase-shift and radial-velocity amplitude. Such an approximation has proved to be useful, e.g., in the case of Cyg X-1 (cf. Figure 7.4 in Hadrava, 2016, and the references therein). This Solution IV (given in Table 1 and displayed in Figure 2) has bit less pronounced emission wings of the primary and instead of it there is a circumstellar emission blob mowing with an amplitude of radial velocity equal to (125.2±0.4) $\mathrm{km\,s^{-1}}$ and ('periastron') longitude $136.8° \pm 0.5°$. The fit of the input spectra is much better, despite it is not yet so precise as in the 'metallic' lines.

4. Conclusion

Our `KOREL` disentangling of spectra of DPV-065 improved the orbital parameters and provided the first spectroscopic evidence of the presence of an accretion disk around the primary star and the circumstellar matter in this system. This interesting system will require a further observational as well as theoretical investigation. In particular, we plan to compare the disentangled spectra with synthetic models.

Acknowledgements. This work has been supported by project GACR 14-37086G. M.C. acknowledges support by the Astronomical Institute of the Czech Academy of Sciences. R.E.M. gratefully acknowledges support by VRID-Enlace 218.016.004-1.0 and the Chilean Centro de Excelencia en Astrofísica y Tecnologías Afines (CATA) BASAL grant AFB-170002.

References

Dekker, H., D'Odorico, S., Kaufer, A., Delabre, B., & Kotzlowski, H., Design, construction, and performance of UVES, the echelle spectrograph for the UT2 Kueyen Telescope at the ESO Paranal Observatory. 2000, in Proc. SPIE, Vol. **4008**, *Optical and IR Telescope Instrumentation and Detectors*, ed. M. Iye & A. F. Moorwood, 534–545

Hadrava, P., FOTEL 4 - User's guide. 2004a, *Publications of the Astronomical Institute of the Czechoslovak Academy of Sciences*, **92**, 1

Hadrava, P., KOREL - User's guide. 2004b, *Publications of the Astronomical Institute of the Czechoslovak Academy of Sciences*, **92**, 15

Hadrava, P., Disentangling of Stellar Spectra. 2016, in Astrophysics and Space Science Library, Vol. **439**, *Astronomy at High Angular Resolution*, ed. H. M. J. Boffin, G. Hussain, J.-P. Berger, & L. Schmidtobreick, 113

Mennickent, R. E., Long Photometric Cycles in Hot Algols. 2017, *Serbian Astronomical Journal*, **194**, 1, DOI: 10.2298/SAJ1794001M

Mennickent, R. E., Otero, S., & Kołaczkowski, Z., Interacting binaries W Serpentids and double periodic variables. 2016, *MNRAS*, **455**, 1728, DOI: 10.1093/mnras/stv2433

Mennickent, R. E., Pietrzyński, G., Diaz, M., & Gieren, W., Double-periodic blue variables in the Magellanic Clouds. 2003, *Astron. Astrophys.*, **399**, L47, DOI: 10.1051/0004-6361:20030106

Poleski, R., Soszyński, I., Udalski, A., et al., The Optical Gravitational Lensing Experiment. The OGLE-III Catalog of Variable Stars. X. Enigmatic Class of Double Periodic Variables in the Large Magellanic Cloud. 2010, *AcA*, **60**, 179